

# Self-Assembly of Semiconductor Nanoplatelets into Stacks Directly in Aqueous Solution

Rebecca T. Graf, Kevin Tran, Marina Rosebrock, Hadir Borg, Jakob Schlenkrich, Franziska Lübkekmann-Warwas, Franz Renz, Dirk Dorfs, and Nadja C. Bigall\*

Since their discovery, cadmium chalcogenide nanoplatelets (NPLs) gained a lot of interest, not only due to their beneficial characteristic, but also because of their high affinity to self-assemble into ordered stacks. Interestingly, the stacks showed both the properties of the single NPLs and new collective features, such as charge carrier transport within the stacks. Until now, the stacking was, to the best of the knowledge, only performed in non-polar media mostly through the addition of antisolvents with higher polarity. Due to the fact, that many applications (e.g., photocatalysis) or procedures (such as gelation) occur in water, a route to self-assemble stacks directly in aqueous solution is needed. In this work a new synthesis route is thus introduced to produce stacks directly in aqueous media. The NPLs are phase transferred with mercaptocarboxylic acids to an aqueous KOH solution followed by an addition of less polar antisolvents to initialize the stacking (e.g., tetrahydrofuran). Furthermore, a mechanism of the stacking as well as four possible driving forces involved in the process are proposed supported by transmission electron microscopy, dynamic light scattering, infrared spectroscopy, and x-ray photoelectron spectroscopy measurements.

## 1. Introduction

It is well known from research, that cadmium chalcogenide nanoplatelets (NPLs) possess an atomically precise growth mechanism and interesting optical properties.<sup>[1–4]</sup> But more important, they show a high affinity to assemble into ordered stacks due to their anisotropic shape.<sup>[5–13]</sup> Furthermore, it was shown that their assembly leads to the rise of interesting collective properties of the stacks compared to the NPLs such as charge carrier transport within the stacks,<sup>[12,13]</sup> an appearance of a phonon coupling emission line at cryogenic temperatures,<sup>[5]</sup> and emission of polarized light.<sup>[6]</sup>

Until now, stacking has been performed in solvents with low polarity (e.g., tetrahydrofuran, THF) mostly through the addition of an antisolvent with higher polarity.<sup>[5–7,12,13]</sup> Prior to the stacking,

the NPLs are stabilized through long aliphatic chains of the ligands on their surface in organic solvents. Through slow addition of an antisolvent (usually a solvent with higher polarity such as ethanol or acetonitrile), the self-assembly is triggered. An interplay of different driving forces leads to the stacking of the NPLs. While the self-assembly into stacks is driven by attractive van der Waals forces between two flat plates, the interaction between the ligands stabilize the stacks.<sup>[9]</sup> Furthermore, one of the driving forces for this assembly is the minimization of the contact area of the non-polar ligands with the polar antisolvent, as repulsive forces between ligand chains can become attractive interactions in the presence of polar antisolvents, known from quantum calculations.<sup>[5,6,9,14]</sup> Hereby, the ligands of neighboring NPLs can intercalate and interact attractively via dispersive forces (usually called hydrophobic interactions) forming a stack in direction of the thickness.<sup>[9]</sup> Between the long aliphatic chains of the ligands (oleic acid, myristic acid) attractive van der Waals forces are stabilizing the formed stacks.<sup>[7]</sup> Thus, the self-assembly is an interplay of different driving forces, such as the van der Waals attraction between flat plates, the contact area minimization with the antisolvent, attractive van der Waals interactions between the ligand chains, balanced with repulsive forces such as the steric potential.<sup>[5–7,9]</sup>


Until now a phase transfer to aqueous medium, as many applications require, was only achieved at the end of the stacking

R. T. Graf, M. Rosebrock, H. Borg, J. Schlenkrich, F. Lübkekmann-Warwas, D. Dorfs, N. C. Bigall  
Institute of Physical Chemistry and Electrochemistry  
Leibniz Universität Hannover  
30167 Hanover, Germany  
E-mail: nadja.bigall@pci.uni-hannover.de

R. T. Graf, K. Tran, F. Renz, D. Dorfs, N. C. Bigall  
Laboratory of Nano- and Quantum Engineering  
Leibniz Universität Hannover  
30167 Hanover, Germany

K. Tran, F. Renz  
Institute of Inorganic Chemistry  
Leibniz Universität Hannover  
30167 Hanover, Germany

R. T. Graf, M. Rosebrock, H. Borg, J. Schlenkrich, F. Lübkekmann-Warwas, D. Dorfs, N. C. Bigall  
Cluster of Excellence PhoenixD (Photonics Optics and Engineering–Innovation Across Disciplines)  
Leibniz Universität Hannover  
30167 Hanover, Germany

 The ORCID identification number(s) for the author(s) of this article can be found under <https://doi.org/10.1002/admi.202300408>

© 2023 The Authors. Advanced Materials Interfaces published by Wiley-VCH GmbH. This is an open access article under the terms of the Creative Commons Attribution License, which permits use, distribution and reproduction in any medium, provided the original work is properly cited.

DOI: 10.1002/admi.202300408

procedure in non-polar solvents through a polymer encapsulation step.<sup>[12,13]</sup> Here, the side chains of the polymer can intercalate between the outer ligands through dispersive forces, leading to a small polymer layer around the stacks.<sup>[9,12,15]</sup> Additionally, the polymer leads to slightly smaller NPL-NPL distances through depletion attraction forces pressing the NPLs closer together.<sup>[12,13]</sup> Nevertheless, this water transfer leads to polymer encapsulated NPL-stacks which are for some applications non-ideal. For example, the electrical conductivity of the stacks is decreased through this non-conductive polymer shell. Furthermore, in other applications such as in catalysis the surface accessibility of the semiconductor often plays a crucial role.

Therefore, the present work focuses on a direct self-assembly of NPL-stacks in aqueous solution (without polymer encapsulation) to open up the possible applications and methods, such as various gelation methods,<sup>[16–19]</sup> ink-jet printing,<sup>[20]</sup> photocatalysis,<sup>[21]</sup> photo-electrochemistry,<sup>[12,13,22]</sup> photodetection<sup>[23]</sup> and sensing,<sup>[24]</sup> light emitting diodes,<sup>[25]</sup> and many more. For this approach CdSe NPLs are first transferred to aqueous solution via ligand exchange to 11-mercaptopundecanoic acid. Secondly, different antisolvents with lower polarity are added to initialize the stacking process and third, dynamic light scattering (DLS) and transmission electron microscopy (TEM) measurements are performed to monitor the stacking amount. Furthermore, an additional purification step after the phase transfer is applied enhancing the amount of stacking significantly. Also, the samples are investigated through X-ray photoelectron spectroscopy (XPS) and infrared-spectroscopy (IR) allowing conclusions about the ligand binding and possible driving forces for the stacking process in aqueous media.

## 2. Results

### 2.1. Phase Transfer of Oleic Acid Capped Nanoplatelets

As previous works have shown, cadmium selenide nanoplatelets possess a great tendency to self-assemble into ordered stacks, which is the reason why we chose them also for this work.<sup>[12,13]</sup> Quasi-quadratic cadmium selenide nanoplatelets (CdSe NPLs) with lateral sizes of  $(14.3 \pm 1.8) \text{ nm} \times (11.8 \pm 1.4) \text{ nm}$  (aspect ratio  $1.22 \pm 0.15$ , derived from TEM micrographs) with narrow size distributions in their lateral dimensions and atomically precise thickness of 4.5 ML (1.2 nm) were synthesized according to literature (Figure S1, Supporting Information).<sup>[4,6,12]</sup> The extinction shows the two characteristic heavy hole-electron and light hole-electron transition signals at 510 and 479 nm, respectively (Figure S2, Supporting Information). In the photoluminescence emission spectrum a narrow emission signal at 515 nm confirms the purity of the 4.5 ML thick oleic acid capped CdSe-NPLs (called OLA-NPLs in the following, Figure S3, Supporting Information).

The as-synthesized OLA-NPLs were phase transferred with 11-mercaptopundecanoic acid (MUA, C<sub>11</sub>) as long chained mercaptocarboxylic acid following a literature route.<sup>[24,26,27]</sup> The phase transfer is based on a ligand exchange reaction from oleic acid (OLA) to the 11-mercaptopundecanoic acid (MUA) as surface ligands. Thereby, the OLA is bound by the acid group as carboxylate to the cadmium terminated NPL surface. Contrary, the MUA is bound with the thiol group to the CdSe surface while the acid group of the mercaptocarboxylic acid stabilizes the NPLs in the

aqueous KOH solution through repulsion forces of the deprotonated carboxylate group, as also known for, e.g., CdSe/CdS core/crown NPLs and CdSe/CdS dot-in-rod structures.<sup>[26]</sup> The phase transfer was carried out in high excess of the MUA in a two-phase system through vigorous shaking overnight. The successful phase transfer was monitored by transfer of the previously in the organic hexane phase dispersed NPLs to the polar methanol phase (Figure S4, Supporting Information). The phase transferred NPLs were precipitated, redispersed in aqueous KOH, and purified by washing with KOH with a centrifuge filter. The MUA-capped CdSe-NPLs (called MUA-NPLs in the following) were used for all further experiments. The extinction and photoluminescence spectra of the phase-transferred MUA-NPLs undergo a bathochromic shift (hh-e: 532 nm), known from literature,<sup>[26,28]</sup> due to the partial delocalization of the exciton over the sulfur head group of the mercaptocarboxylic acids (Figures S2 and S3, Supporting Information).

### 2.2. Stacking Procedure for Mercaptopundecanoic Acid Capped CdSe Nanoplatelets

To initialize the self-assembly of the MUA-NPLs a similar procedure to the OLA-NPL system was tested (Figure 1).

For aqueous MUA-NPLs, the effect of an addition of antisolvents with less polarity than water was monitored with transmission electron microscopy (TEM) and dynamic light scattering (DLS). Different antisolvents such as methanol (MeOH), ethanol (EtOH), acetonitril (ACN), and tetrahydrofuran (THF) with decreasing polarity (MeOH > EtOH > ACN > THF) were tested. Further, various NPL dispersion to solvent ratios (1:0.33, 1:0.66, 1:1, 1:2,  $V_{\text{NPLs}}:V_{\text{antisolvent}}$ ) were examined, and can be seen in Figure 2 and Figure S6 (Supporting Information). Here, the starting concentration and volume of the original NPL solution was kept constant while different amounts of antisolvent were slowly added (see Experimental Section).

Thereby, the DLS measurements can give insight into the hydrodynamic sizes of the dispersions without distinguishing between ordered stacking and non-ordered agglomeration, while the TEM micrographs of the drop casted dispersions can monitor the stacking in the dried sample. Furthermore, it should be noted, that for DLS Brownian molecular motion of spherical particles is assumed, while here the NPL possess an anisotropic shape. Nevertheless, while the exact values should be used with caution, DLS can give valuable information about the status of the self-assembly process. To analyze the influence of the antisolvents on the stacking, both methods, DLS and TEM, will be combined to best depict the assembly in solution. In the TEM micrographs, the stacking can be monitored through NPLs standing on their sides (visible as parallel dark stripes) or overlapping parallel laying NPLs, which seem to have fallen over during the drying process. Furthermore, it should be noted that slow solvent evaporation can also initialize the stacking process as shown in literature.<sup>[5,10]</sup> Nevertheless, here the solution was dropped on the TEM grid in a fashion, that most of the liquid was absorbed into the underlying filter paper to prevent a slow drying process. The TEM images of the non-destabilized MUA-NPL sample indeed only show a negligible amount of stacking and mostly have NPLs laying flat on the grid (Figure S1,

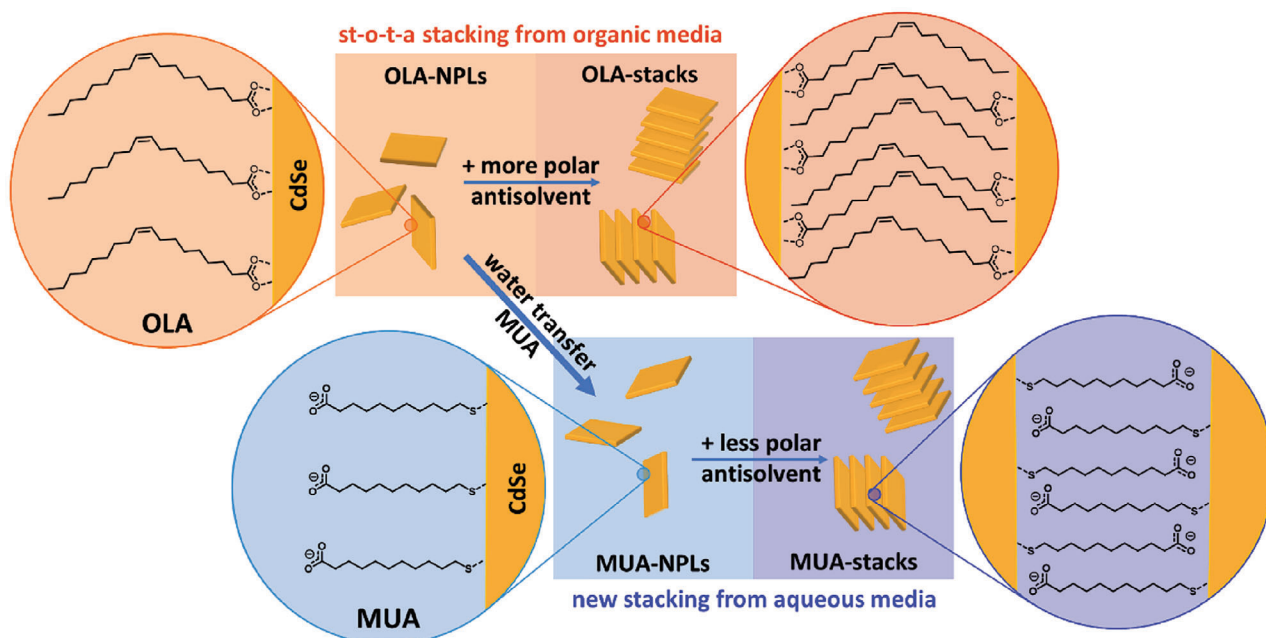


**Figure 1.** Schematic description of the state-of-the-art stacking mechanism of oleic acid capped CdSe-NPLs (called OLA-NPLs, top) from non-polar medium and the new stacking method of 11-mercaptoundecanoic acid capped CdSe-NPLs (called MUA-NPLs, bottom) from polar (aqueous) medium. The addition of an antisolvent with different polarity than the solvent initializes the stacking, while different van der Waals forces (between the flat NPLs; and between the intercalated ligands) stabilize the formed stacks. The MUA-NPLs were synthesized from the OLA-NPLs through a water transfer with MUA.

low magnification in Figure S5, Supporting Information). Therefore, the solvent evaporation as stacking initiation seems to be no prominent process in this preparation and thus will not be considered further.

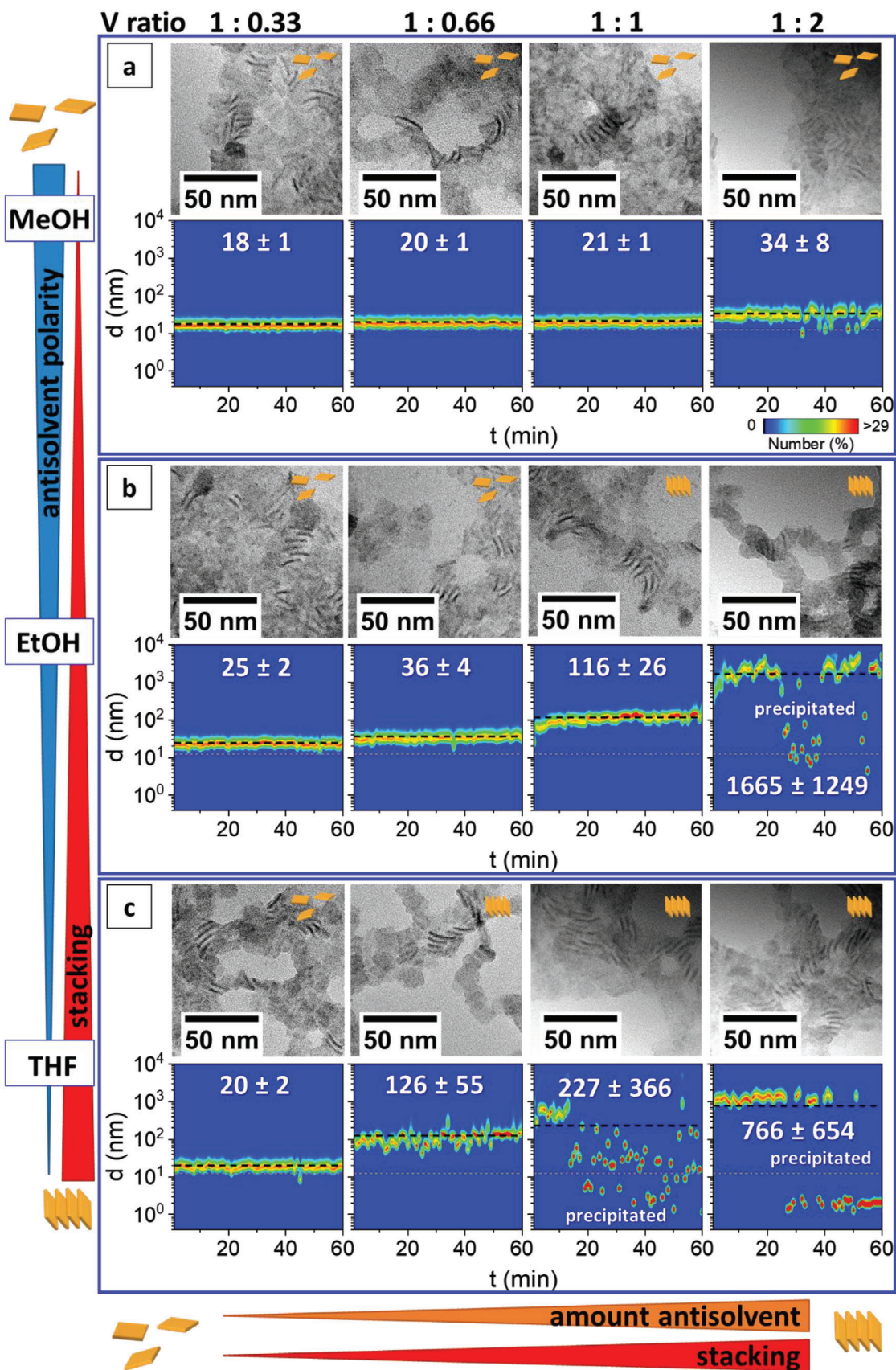
The as-synthesized MUA-NPLs mostly lay flat on the TEM grids and show a hydrodynamic radius of  $(12 \pm 1)$  nm in the DLS, fitting to the lateral dimensions of  $\approx 14$  nm x 12 nm (1.2 nm thickness) measured by TEM micrographs (Figure S5, Supporting Information). Starting with this stable solution ( $c_{Cd} = 19.57$  mmol L<sup>-1</sup>) the additions of certain amounts of different solvents were monitored in the DLS for 1 h each with one measurement per minute. The numbers size distribution spectra were depicted as 3D plots over the time, to not only show the mean values, but also the size distribution (Figure 2; Figure S6, volume and intensity size distributions can be found in Figures S10 and S11, Supporting Information). For MeOH, which has the least polarity difference to water, even the highest amounts seem to induce neither a significant increase in the hydrodynamic radius nor a mentionable amount of stacking in the TEM micrographs (Figure 2a, lower magnification TEM micrographs are in Figures S7–S9, Supporting Information). In contrary, THF, which had the highest tested polarity difference, shows prominent self-assembly already for a 1:0.66 NPL solution to antisolvent ratio ( $V_{NPLs} \cdot V_{antisolvent}$ ) through a high hydrodynamic radius of over 100 nm (Figure 2c). The TEM micrographs of this sample thereby verify the ordered assembly of the NPLs into stacks through parallel standing NPLs and overlapping parallel fallen NPLs. Furthermore, as no prominent increase of the assemblies is visible in the DLS data over 60 min, the self-assembly seems to be completed already after the first minute of the measurement. This shows that the self-assembly is a fast process, most probably

happening on the time scale of seconds. A lower amount of THF (1:0.33,  $V_{NPLs} \cdot V_{antisolvent}$ ) seems to be insufficient as driving force to initiate a large amount of stacking, which can be seen in the TEM micrograph of mostly random laying NPLs and a hydrodynamic radius of 19 nm.

For the solvents with higher polarity difference than MeOH, the higher the amount of antisolvent, the higher is the amount of stacking visible in the TEM micrographs (Figure 2b; Figure S3, Supporting Information, left to right). The DLS measurements shows the same trend as the TEM micrographs of increasing hydrodynamic radii with increasing antisolvent amount until the assembled MUA-stacks were not stable in the solvent-antisolvent mixture anymore and precipitated completely (photograph Figure S12, Supporting Information). Furthermore, a trend of increasing amount of stacking with increasing polarity difference between antisolvent and solvent (polarity difference: MeOH < EtOH < ACN < THF) is visible.

For oleic acid capped CdSe-NPLs (called OLA-NPLs) dispersed in THF it is known, that solvents with higher polarity, such as EtOH and ACN, act as antisolvents).<sup>[5,6]</sup>

For better comparison, the original OLA-NPL system was also analyzed in TEM and DLS with the according antisolvents and solvent to NPL ratios (Figure S17, Supporting Information). In the case of OLA-NPLs the stacking is initiated through the addition of a destabilization agent which has a higher polarity than the solvent (polarities: MeOH > EtOH > ACN > THF). For OLA-stacks the expected trend – the higher the polarity of the antisolvent and thus the higher the polarity difference between antisolvent and solvent, the higher is the amount of stacking visible in the TEM micrographs – was observed indeed (Figure S17, Supporting Information). The DLS



measurements are fluctuating a lot and thus not analyzed any further.

In summary, for both systems MUA-NPLs and OLA-NPLs the same trend is visible: the larger the polarity difference between solvent and antisolvent, the higher is the amount of stacking. This is in good agreement with the literature for the known system of the organic OLA-NPLs and can obviously be transferred to the aqueous MUA-NPLs. To understand those trends more in detail, the ligand interactions which play a crucial role in the stacking procedure are analyzed further in the following section.

### 2.3. Driving Forces of Ordered Stacking

To understand the different driving forces of the stacking mechanism in the new aqueous MUA-NPL system, the known OLA-NPL system will be used as starting point. In general, the lowering of the free energy of the system can be seen as the overall driving force of the self-assembly.<sup>[29]</sup> Thereby, the free energy evolution of the system is a summation of multiple energies in the system such as the energy of the interaction of parallel plates, the free energy of the chain-solvent mixing, as well as the inter-chain interaction energy of the ligands.<sup>[29]</sup> To simplify the discussion, we will address them as attractive and repulsive interactions which combine to the effective interparticle pair interaction (an in depth discussion of self-assembly processes can be found in a review from Boles et. al.).<sup>[29]</sup>

As already stated, the driving forces for the stacking mechanism are highly complex, as there are a multitude of different attractive and repulsive interactions which can furthermore change during the process.<sup>[29,30]</sup> The prominent forces in the NPL solution are thereby attractive van der Waals forces between the NPLs themselves and repulsive interactions of the surface ligands.<sup>[9,29,30]</sup> The van der Waals forces of this surfaces with low curvature would lead to a stacking of the NPLs while in a good solvent the repulsive forces overcome the attractive van der Waals forces leading to a stable NPL solution.<sup>[9,29,30]</sup> The steric interactions are based on osmotic repulsion and elastic repulsion.<sup>[29]</sup> Thereby, the osmotic repulsion results from solvent molecules being separated from the ligands when particles approach each other and ligands overlap, losing attractive solvent-ligand interactions.<sup>[29]</sup> The elastic component results from compression of the ligands at small distances.<sup>[29]</sup>

For OLA-NPLs the ligands are bound as deprotonated carboxylates to the Cd-terminated NPL surface while the aliphatic chains of the OLA ligands stabilize the NPLs in organic solvents (as good solvent). The stacking can be initialized through different methods, which decrease the repulsive interactions leading to an overall attractive force forming the stacks. In example, the reduction of the solvent quality (by addition of antisolvents or by cooling) as well as solvent evaporation or ligand removal or cross-linking of ligands can initialize the stacking.<sup>[29]</sup> Here, for OLA-

stacks, the addition of the antisolvent (e.g., ethanol EtOH, acetonitrile ACN) with higher polarity than the solvent (e.g., tetrahydrofuran THF) can act as driving force for the stacking. More precisely, the driving force can be attributed to the minimization of the contact area between the organic aliphatic chains of the ligands and the polar antisolvents.<sup>[5,6]</sup> Furthermore, it was shown in quantum calculations, that repulsive ligand interactions can become attractive ones in the presents of polar solvents (as bad solvents).<sup>[9,29,30]</sup> Driven by the antisolvent addition, the oleic acid chains of neighboring OLA-NPLs are expected to intercalate (indicated by inter-NPL distances of less than two fully stretched ligands), which are known as dispersive forces and hydrophobic interactions.<sup>[9,12,29,30]</sup> Thereby, the stacks are stabilized through attractive van der Waals forces between the intercalated long aliphatic ligand chains (oleic acid C<sub>18</sub>) acting as an additional driving force (Figure 1).<sup>[7,9,29,30]</sup> Previously, it was also shown that polymers with aliphatic side chains could lead to smaller inter-NPL distances due to an additional depletion force pressing the NPLs closer together.<sup>[12]</sup> Furthermore, it was shown that a smaller amount of long steric ligands would decrease the distance between the NPLs due to easier intercalation.<sup>[13]</sup>

In summary, the anisotropic shape of the OLA-NPLs and their low curvature and with this the attractive van der Waals forces between flat surfaces, together with the maximal overlap of ligands and thus van der Waals attraction between the ligands, lead to the ordered assembly in form of stacking in direction of their thickness. The stacking is initialized as soon as the steric repulsive forces of the ligands are overcome. Here, the addition of antisolvents act as this initiator favoring the minimization of the contact area between antisolvent and ligands.<sup>[9,29,30]</sup>

For MUA-NPLs the same attractive van der Waals forces between flat surfaces should favor ordered assembling into stacks while the repulsion interactions of the MUA ligands stabilize the NPLs in solution. Nevertheless, the binding situation of the MUA ligand is different than the oleic acid and hence, the stabilization of the formed stacks through ligand interactions should be different as well. The 11-mercaptoundecanoic acid is known to bind via the sulfur of the former thiol group to the cadmium terminated CdSe-NPL surface building a Cd-S bond.<sup>[24,26,27]</sup> This was also verified in this work through XPS and FTIR and is discussed later on. Further, the acid groups of the MUA stabilize the MUA-NPLs in an aqueous KOH solution via charge repulsion of the deprotonated carboxylate end groups between different NPLs.<sup>[26]</sup> Thus, not only the steric stabilization of the long aliphatic chains, but also the electrostatic stabilization of the charged end groups (the combination also called electrosteric stabilization) needs to be overcome to initialize the stacking process.<sup>[29]</sup>

Taking those binding situations into account, the following driving forces for the stacking mechanism from aqueous solution could be derived (visualized in Figure 3) and need to be investigated in the following:

**Figure 2.** TEM images of 11-mercaptoundecanoic acid capped CdSe-NPLs (called MUA-NPLs) from aqueous KOH ( $10^{-2}$  M) after the addition of anti-solvents with different polarity, a) MeOH, b) EtOH, c) THF, and varying NPLs to antisolvent volume ratios (1:0.33, 1:0.66, 1:1, 1:2,  $V_{\text{NPLs}}:V_{\text{antisolvent}}$ , left to right, lower magnification TEM in Supporting Information). Hydrodynamic sizes of the assemblies measured for 60 min after antisolvent addition with a gray line indicating the mean value of MUA-NPLs (12 nm) before addition and a black line indicating the mean value after antisolvent addition (derived by the numbers size distribution of dynamic light scattering, DLS, volume and intensity size distribution are in the Supporting Information). For MUA-NPLs in KOH the size of the assemblies (measured by the hydrodynamic size) and the amount of stacking (visible in the TEM micrographs) increases with decreasing antisolvent polarity and increasing antisolvent amount.

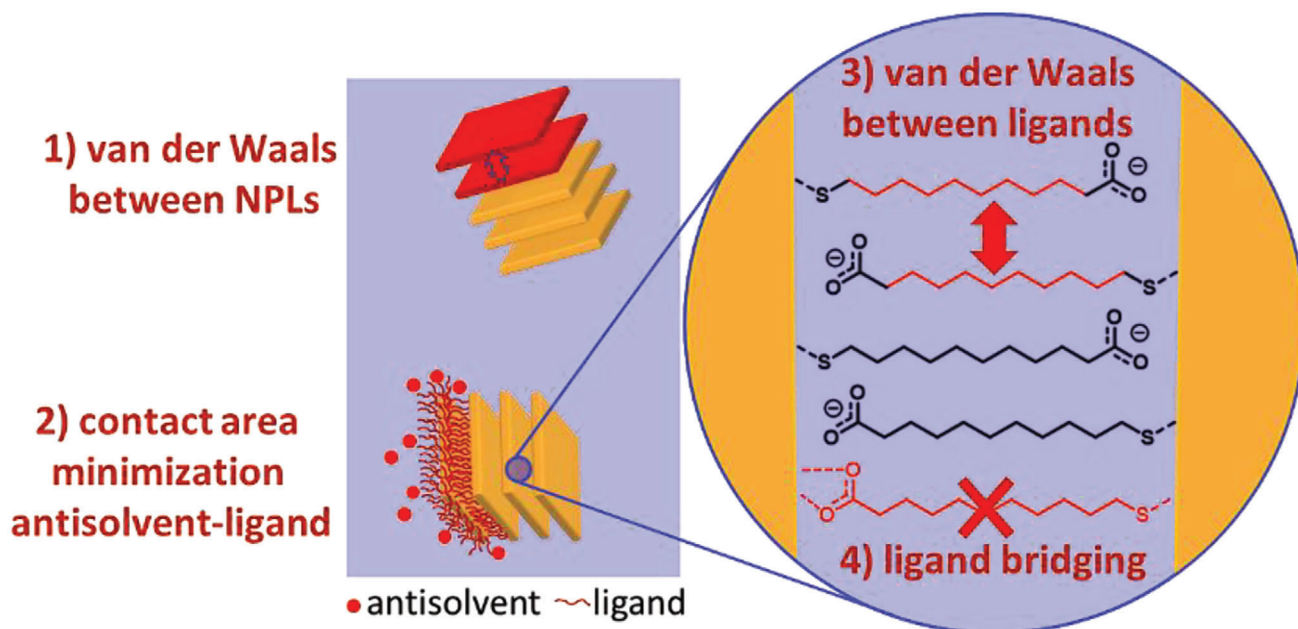


**Figure 3.** Visualization of different possible driving forces for the stacking process in aqueous media, initiated by the addition of less-polar antisolvents: 1) Van der Waals attraction between NPLs; 2) Contact Area minimization between ligands and antisolvents; 3) Van der Waals attraction between intercalated ligands; 4) Bridging of NPLs through ligands.

- 1) Van der Waals attraction between NPLs: Attractive van der Waals forces between the flat surfaces of the NPLs lead to the formation of stacks, when the repulsive forces are smaller, and thus, are a strong driving force for the self-assembly.
- 2) Contact Area minimization between ligands and antisolvents: In the stacking procedure, the electrosteric repulsion of the long aliphatic ligands with the charged carboxylate end groups needs to be overcome, for the ligands to intercalate and form ordered stacks. Here, the polarity difference between antisolvent and solvent could act as a possible driving force by minimizing the contact area between the charged ligands and the non-favorable non-polar antisolvent. Further, a possible protonation of the carboxylate end groups is thinkable to diminish the charge repulsion between the ligands and thus should also be considered.
- 3) Van der Waals attraction between intercalated ligands: When the repulsion of the carboxylate end groups is overcome, the aliphatic chains of neighboring MUA-NPLs can intercalate. Hereby, the stacks could be stabilized through attractive van der Waals forces between the aliphatic ligand chains, which could be considered as third driving force for the ordered assembly.
- 4) Bridging of NPLs through ligands: A ligand bridging of two neighboring MUA-NPLs through the mercaptocarboxylic acid ligands (possessing two functional end groups) could be possible. Thereby, a binding of the MUA ligand, which is bound via the sulfur group to one NPL (Cd-S), to the neighboring Cd-terminated NPL via the carboxylate end group could be thinkable. This could be possible when the distance between the NPLs is small enough, as COO-Cd bond are known to form for carboxylic acids on CdSe (e.g., CdSe-OLA).

To validate those hypotheses, different characterization methods such as XPS and FTIR together with measurements of the inter-NPL distance derived from high resolution TEM micrographs were carried out.

### 2.3.1. Van der Waals Attraction between NPLs

As described for the OLA-NPLs, attractive van der Waals forces act between the NPLs. Due to their low curvature and anisotropic shape, the van der Waals interactions between the flat plates would assemble the NPLs into stacks as soon as the repulsive forces of the ligands are overcome.<sup>[9,29,30]</sup> The theory and calculations of the van der Waals forces are quite complex, as they depend, e.g., on the electron distribution (e.g., large in metals) as well as the area and thus the curvature of the particles.<sup>[29,31]</sup>

Nevertheless, as neither the material, nor the size and curvature of the CdSe-NPLs change significantly during the phase transfer, the interparticle interaction between the MUA-NPLs should be comparable to the interaction in the OLA-NPLs. Therefore, it can be assumed, that the van der Waals attraction between the NPLs is as well an important driving force of the assembly in aqueous solution.

### 2.3.2. Contact Area Minimization between Ligands and Antisolvents

Repulsive interactions of the steric ligands in a good solvent are known to become attractive interactions in a bad solvent, as stated for the OLA-stacks previously.<sup>[5,6,9,29,30]</sup> This can also be described as preferred contact area minimization between ligand and the bad solvent. For the MUA ligands the charged carboxylate end

groups leads to not only steric but also electrostatic repulsions, named electrosteric repulsion, which needs to be diminished.<sup>[29]</sup>

The previously described TEM and DLS results showed, that the addition of antisolvents with large polarity difference indeed seems to be efficient to overcome the repulsion between the ligands. Thus, the antisolvent addition can act as driving force (2) for the assembly (similar to the conventional OLA system) through a controlled destabilization of the NPL dispersion. More precisely, the contact area minimization between the less polar antisolvents and the charged MUA ligands is most probably the driving force in this process. The trend of higher amounts of stacking with higher polarity difference between solvent and antisolvent, as well as the trend of higher stacking amounts with higher antisolvent amounts as described earlier are in good accordance with this hypothesis.

Additionally, a protonation of the carboxylate end groups would be expected to reduce the charge repulsion between the electrosteric ligands and thus could probably help to initialize the stacking. To validate this part of the hypothesis, the state of deprotonation was monitored via XPS measurements (Figure 4).

Thereby, the C 1s signal of pure MUA shows a signal at 284.73 eV, which can be assigned to C<sup>\*</sup>-C/C<sup>\*</sup>-H,<sup>[32]</sup> at 289.23 eV associated to C<sup>\*</sup>OOH, and at 285.37 eV correlated to C atoms in the close proximity of the acid or thiol group.<sup>[32]</sup> All XPS fit data such as peak positions and areas are listed in Tables S1 – S4 (Supporting Information). When the pure MUA ligands are dissolved in an aqueous KOH solution, the signal of the carboxyl group shifts to lower binding energies at 287.99 eV. This can be allocated to carbon of the deprotonated carboxylate group C<sup>\*</sup>OO<sup>-</sup>, as the deprotonation leads to higher electron density at the oxygen atoms and thus the electrons of the carbon are less drawn to the oxygen atoms and more loosely bound leading to lower binding energies.<sup>[32,33]</sup>

With these assignments as references, the MUA-NPLs and -stacks can be analyzed. The MUA-NPLs and -stacks both show an additional signal at low binding energies at 282.89 eV which was already seen in literature for carbon atoms in close proximity to metal atoms and thus can be assigned to carbon atoms close to the Cd-bound thiol group.<sup>[34,35]</sup> In the MUA-NPLs the C<sup>\*</sup>OO<sup>-</sup> signal is visible at 288.07 eV. For the MUA-stacks to distinguish between the stacks and free ligands in the solution, an additional precipitation of the stacks after the THF addition (4226 rcf, 1 min) was performed and the precipitate (containing the stacks, called MUA-stacks-precipitate) and the supernatant (containing the free ligand, named MUA-stacks-supernatant) were measured separately. The MUA-stacks-supernatant shows a mixture of the pure MUA and MUA-KOH samples having both C<sup>\*</sup>OOH (289.19 eV) and C<sup>\*</sup>OO<sup>-</sup> (287.91 eV) signals and no NPL signals (Figure 4). On the other hand, the precipitated MUA-stacks (MUA-stacks-precipitate) have the same signals as the MUA-NPLs having only the C<sup>\*</sup>OO<sup>-</sup> signal present at 288.11 eV, showing no detectable protonation of the acid group. The O 1s signal on the other hand is quite difficult to analyze having no distinct signals but a broad convoluted signal as known for CdSe/CdTe NPLs capped with OLA (Figure S18, Supporting Information).<sup>[36]</sup> The O 1s fitting would lead to a contrary result of more protonation in the stacks (see Section S4, Supporting Information). However, due to the difficult analysis of the O 1s signals they should not be relied on for the interpretation, while the C 1s

signals should be more accurate (having distinct peaks) about the state of the deprotonation of the ligands. Nevertheless, even if the ligands are partially protonated in the process (as the O 1s signal could suggest), the antisolvent addition still needs to overcome the repulsion of the electronegative acid/carboxylate end groups of neighboring NPLs in the stacking process.

As the stacking does indeed occur after the antisolvent addition, the driving force of the stacking must be stronger than the charge repulsion of the carboxylate/acid end groups. Thus, the minimization of the contact area between the ligands and the antisolvent seems to be a strong enough driving force to overcome the charge repulsion as first step in the ordered stacking.

### 2.3.3. Van der Waals Attraction between Intercalated Ligands

To validate (3), the van der Waals forces between the ligands as driving force for the ligand intercalation leading to ordered stacking of the NPLs, the experiments were repeated with the short chained 3-mercaptopropionic acid (MPA, C<sub>3</sub>) ligand. Van der Waals forces depend on the surface area due to the fact, that those regulate the possible interaction with neighboring molecules.<sup>[37]</sup> Thus, short chained aliphatic ligands such as MPA (C<sub>3</sub>) should have significantly weaker attractive van der Waals forces compared to the long chained MUA (C<sub>11</sub>), due to their smaller surface area.<sup>[37]</sup>

The TEM micrographs and DLS 3D plots of MPA-NPLs are shown in Figure 5 and Figure S13 (Supporting Information). The experiments were carried out with THF as antisolvent with highest polarity difference (as THF was inducing the highest amount of stacking for the long-chained MUA system). Here, for MPA-NPLs, the addition of THF indeed leads to a self-assembly visible by the hydrodynamic radius of >1000 nm in the DLS measurement of a 1:1 NPL to THF ratio. Nevertheless, the TEM micrographs reveal no formation of ordered stacks, but of a non-ordered random assembly into MPA-agglomerates (Figure 5b). Due to the anisotropic shape of the NPLs, the highest overlap of long chained ligands and thus the presence of the maximal attractive van der Waals forces occurs when the NPLs are stacked with their lateral areas parallel to each other and thus the highest amount of intercalation of the ligands. However, the TEM micrographs of the destabilized MPA-agglomerates show random self-assembly with NPLs laying flat on the TEM grids connected via corners or edges and mostly no complete overlap as seen in the MUA-stacks. This indicates that our hypothesis (3) is correct, namely the necessity of longer chained ligands and thus larger attractive van der Waals forces between ligands of neighboring NPLs, which seem to be the key driving force to initiate the ordered stacking versus non-ordered agglomeration (Figure 5a).

### 2.3.4. Bridging of NPLs through Ligands

To validate (4) the existence of ligands bridging two NPLs (CdS-(CH<sub>2</sub>)<sub>10</sub>-COO-Cd) bound via their two functional end groups, i.e., the thiol group and the carboxylate group to the neighboring NPLs as driving force for the stacking, XPS and FTIR measurements were carried out. Additionally, inter-NPL distances were measured from high resolution TEM images from surface-to-surface of neighboring NPLs. If the ligands are bridging the

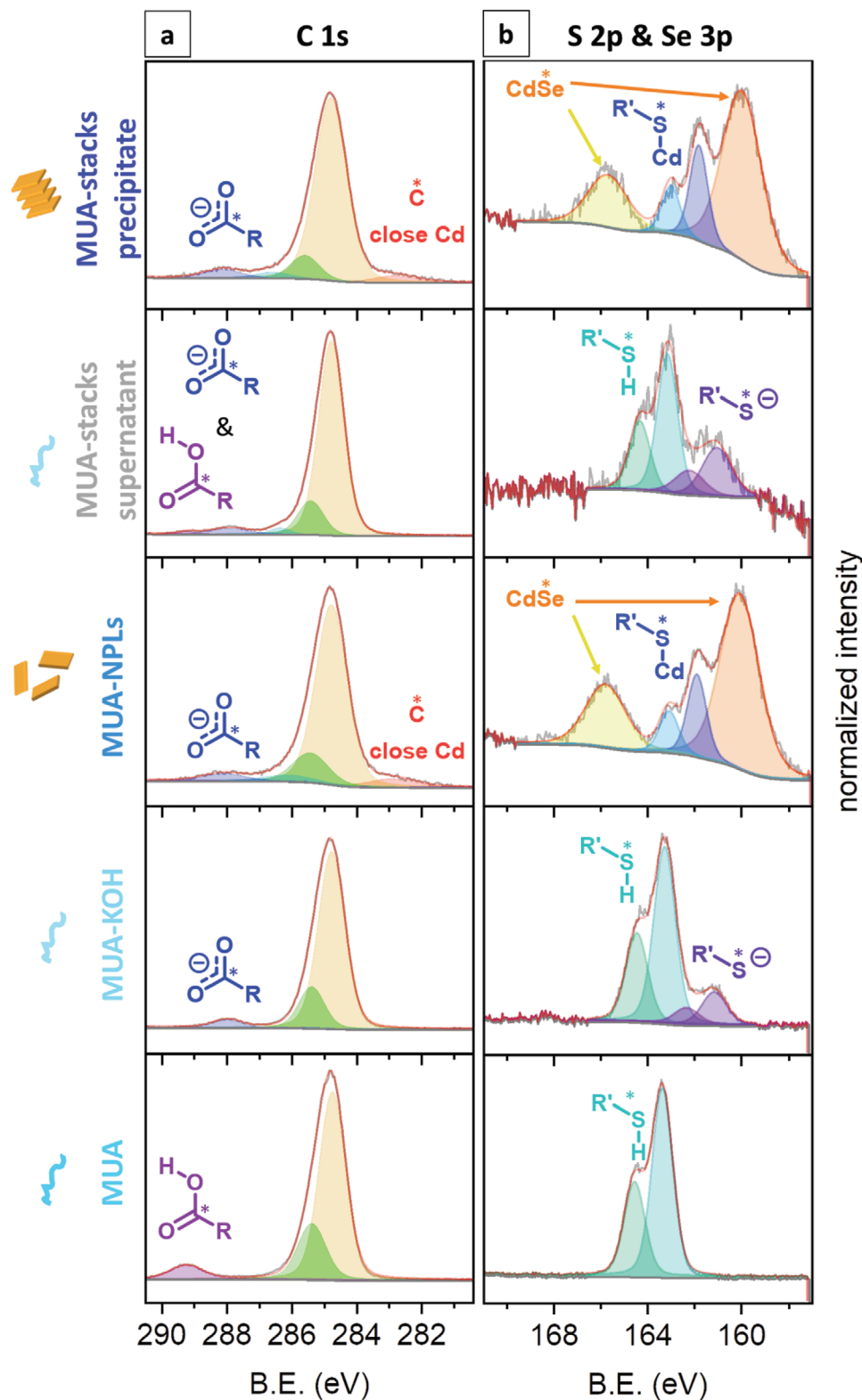


**Figure 4.** High resolution X-ray photoelectron spectroscopy (XPS) measurements of a) the C 1s region and b) the S 2p & Se 3p region of the MUA-NPLs and pure MUA ligands as well as a mixture of MUA and MeOH-KOH. The MUA-stacks after destabilization with THF as antisolvent (1:1,  $V_{\text{NPLs}}:V_{\text{antisolvent}}$ ) were precipitated to separate the stacks (MUA-stacks precipitate) from free ligands in the supernatant (MUA-stacks supernatant). While the MUA-NPLs and MUA-stacks (precipitate) possess carbon close to Cd and mostly deprotonated carboxylate ligands, the supernatant shows solely signals of free MUA ligands. In the MUA-NPLs and MUA-stacks (precipitate), the ligands are bound via their deprotonated thiol group to the Cd surface forming a Cd—S—R bond. A more detailed analysis of the signals is done in Tables S1–S4 (Supporting Information).



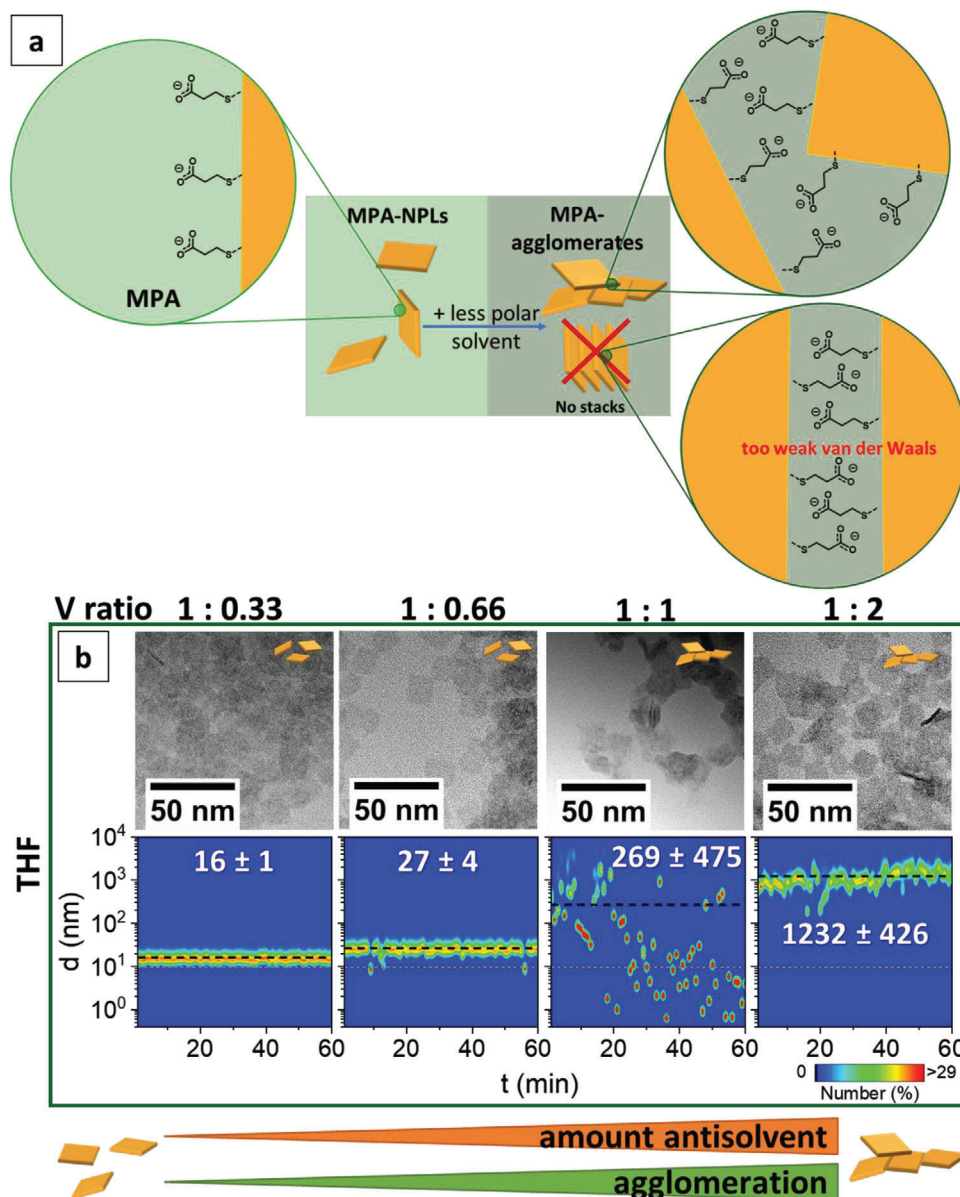


**Figure 5.** a) Schematic mechanism of the destabilization of 3-mercaptopropionic acid (MPA) capped CdSe-NPLs (called MPA-NPLs) in KOH leading to non-ordered agglomerates instead of stacks, due to insufficient van der Waals forces between the short ligands. b) TEM micrographs and DLS measurements of MPA-agglomerates with different NPL to THF volume ratios (1:0.33, 1:0.66, 1:1, 1:2,  $V_{\text{NPLs}}:V_{\text{antisolvent}}$ ). While, with increasing THF amount, the hydrodynamic radius hints toward the occurrence of larger entities, which could be assembly of the MPA-NPLs, the TEM reveals that this is only due to non-ordered agglomeration. The mean values over 60 min before THF addition (10 nm) is visible as gray dotted line and after THF addition as black dashed line.

neighboring NPLs via their sulfur head group and their acid head group on either side the inter-NPL distance should be smaller or equal the fully stretched ligand length plus the radius of the bond between Cd-terminated NPL surface and the ligand head groups. The fully stretched ligand length was estimated via the Tanford formula<sup>[38]</sup> being  $\approx 1.5$  nm for MUA ( $C_{11}$ ) (Equation S1, Supporting Information). For the MUA-stacks destabilized with the highest tested ratio of 1:2 NPL solution to THF, the inter-NPL surface-to-surface distance was measured to be  $\approx (1.5 \pm 0.3)$  nm (30 measured) which would allow bridging of ligands.

More importantly, the XPS and FTIR measurements give insight into the binding situation of the mercaptocarboxylic acids through the influence of their binding partners on their binding energy or their vibrational modes, respectively. The XPS fits can be found in Figure 4 and Figures S18–S24 (Supporting Information), while all XPS fit data can be found in Tables S1–S4 (Supporting Information). The FTIR spectra of the pure ligands, the pristine NPLs and the stacks (destabilized NPLs with THF) are visible in Figure 6 and Figures S29–S33 (Supporting Information). The band locations and assignments are listed in Table S5 (Supporting Information).

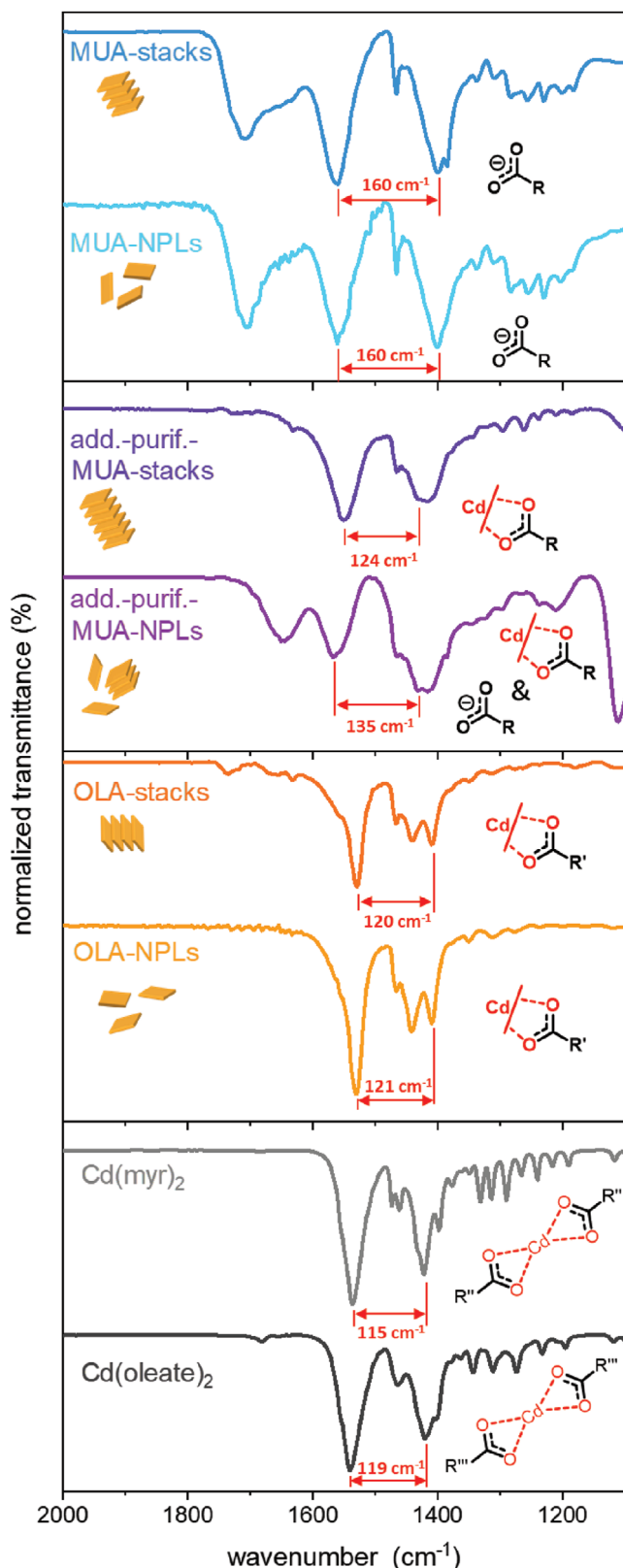


**Figure 6.** Enlarged detail of FTIR measurements of the differently capped NPLs before and after destabilization with antisolvents (MUA-stacks 1:1 THF  $V_{\text{NPLs}}:V_{\text{antisolvent}}$ , add.-purif.-MUA-stacks 1:1 THF, OLA-stacks 1:2 MeOH) as well as ATR measurements of references with bound cad-

mium (cadmium myristate, cadmium oleate). The large distance between the asymmetric and symmetric carboxylate stretch of the MUA-NPLs and MUA-stacks shows no cadmium chelating/bidentate bond. Contrary, the additional purified MUA-stacks (add.-purif.-MUA-stacks) possess a small difference similar to the Cd bound OLA-NPLs, OLA-stacks, and references suggesting a certain amount of ligand bridging via chelating/bidentate bound carboxylate groups to Cd. The complete IR spectra as well as the assignments can be found in Figures S29–S33 and Table S5 (Supporting Information).

As previously mentioned, MUA is expected to bind via the sulfur head group to the Cd-rich CdSe-NPL surface building a Cd-S-R species.<sup>[24,26,27]</sup> This can be monitored through XPS and IR measurements. The XPS of the pure MUA shows a binding energy of 163.33 eV for the S 2p 3/2 (1.19 eV doublet separation to S 2p 1/2, used as constrain for all other S 2p 1/2 fittings) assigned to R-S-H in good comparison to literature of thiols (Figure 4).<sup>[39]</sup> The addition of KOH should partially deprotonate the mercapto-carboxylic acids forming R-S<sup>-</sup>, which is indeed visible in the XPS through an additional sulfur doublet signal shifted to lower binding energies (S 3p 3/2: 161.1 eV) compared to the protonated H-S-R doublet still at 163.23 eV (S 2p 3/2). This shift results from the higher electron density at the sulfur atom in the negatively charged species and the resulting lower binding energies of those loser bound electrons in the XPS measurement. When the MUA is bound to the CdSe-NPLs via R-S-Cd the S signals should be shifted to smaller binding energies compared to R-S-H,<sup>[32,39]</sup> due to the lower electronegativity of the Cd compared to H, but less pronounced shifted than for R-S<sup>-</sup> in MUA-KOH. This expected behavior can be seen in both the MUA-NPL and MUA-stacks sample with the S 2p 3/2 signals shifted to 161.84 eV and 161.73 eV, respectively. The signals so indeed shifted to binding energies in between the protonated R-S-H ( $\approx 163.3$  eV MUA) and the deprotonated R-S<sup>-</sup> ( $\approx 161.1$  eV MUA-KOH) species. This is in good agreement to literature values of 161.3 eV for MUA bound to Cu-In-Zn-S nanoparticles via the metal sulfur bond (reference is charge corrected of C 1s to 284.6 eV).<sup>[32]</sup> Additionally, the Se 3p 3/2 signal of the CdSe-NPLs can be seen in the same region at 160.01 eV (5.76 eV doublet separation to Se 3p 1/2) in all CdSe samples.

Further, in the FTIR spectra the S-H vibration of the pure MUA at 2552 cm<sup>-1</sup> vanishes in the MUA-NPLs and MUA-stacks when the thiol binds to the NPLs via a Cd-S bond (Figure S29, Supporting Information). A signal at 669 cm<sup>-1</sup> in the MUA-NPLs (MUA stacks: 669 cm<sup>-1</sup>) can be assigned to Cd-S vibrations known from CdS nanoparticles around 665 cm<sup>-1</sup>.<sup>[40–42]</sup> So both the XPS and IR verify the binding of the MUA to the CdSe-NPLs in the MUA-NPLs and MUA-stacks through the former thiol head group by the formation of R-S-Cd species being in accordance with literature.<sup>[24,26,27]</sup> Hence, to monitor the possible bridging of NPLs in the MUA-stacks through the MUA ligand forming a Cd-S-(CH<sub>2</sub>)<sub>10</sub>-COO-Cd species, the formation of a carboxylate species bound to Cd needs to be monitored.

For the OLA-NPLs it is known from literature that the ligands are bound via the deprotonated carboxylate group to the Cd terminated NPLs and thus OLA-NPLs will be used as reference.<sup>[5,13,43]</sup> This can be seen in the FTIR through multiple signals (Figure 6; Figure S32, Supporting Information). First, in the IR, on the one hand, the prominent COOH vibration at 1709 cm<sup>-1</sup> as well as

the OH broad band between 3300 and 2500  $\text{cm}^{-1}$  of the pure OLA (known from literature<sup>[44]</sup>) are rapidly decreased in the OLA-NPLs and OLA-stacks. On the other hand, for the OLA-NPLs (and OLA-stacks) the asymmetric and symmetric  $\text{COO}^-$  vibrations appear at 1531 and 1410  $\text{cm}^{-1}$  (OLA-stacks: 1530 & 1468  $\text{cm}^{-1}$ ), respectively, verifying the deprotonation of the acid group when OLA is bound to the NPLs.<sup>[43,45]</sup>

For MUA-NPLs the same decreasing COOH band of pure MUA at 1701  $\text{cm}^{-1}$  and appearing  $\text{COO}^-$  bands in MUA-NPLs at 1560 and 1400  $\text{cm}^{-1}$  (MUA-stacks: 1560 & 1400  $\text{cm}^{-1}$ ) are visible (Figure 6; Figure S29, Supporting Information). Nevertheless, this only shows the expected deprotonation of the carboxylate group due to the KOH and gives no information about the occurrence of bridging. Carboxylates can be bound either by forming a monodentate bond (one oxygen bound to a Cd atom) or a chelate (both oxygens bound to the same Cd) and/or bidentate bond (both oxygen bound to different cadmium atoms) or a mixture of those (generally referred to as Cd–OOC in the following).<sup>[45–47]</sup> To distinguish between a free carboxylate group and a Cd–OOC bond, the difference between the asymmetric and symmetric  $\text{COO}^-$  signal was shown to be useful,<sup>[45–47]</sup> as a study about acetate complexes used this difference to distinguish between either chelating, and bridging or monodentate bound carboxylates.<sup>[46]</sup> For bridging and chelating differences significantly less than the ionic (<150  $\text{cm}^{-1}$ ) were found, while bridging leads to differences above the ionic (>300  $\text{cm}^{-1}$ ) with the differences for the ionic between 160–170  $\text{cm}^{-1}$ .<sup>[46]</sup> Those exact values should not be transferred from acetoacetates directly to any carboxylate ions and thus should be used cautiously. For the OLA-NPLs the difference between asymmetric and symmetric carboxylate vibration is 121  $\text{cm}^{-1}$  (OLA-stacks: 120  $\text{cm}^{-1}$ ) similar to the literature value of 120  $\text{cm}^{-1}$  of OLA bound to aluminum oxide nanoparticles via chelate or bidentate bonds.<sup>[45]</sup> To determine the binding situation in our system, known cadmium carboxylates possessing a chelate bond (both carboxylate oxygen bound to the same Cd atom) were measured in the ATR to get a better insight into the Cd–OOC system (Figure 6; Figure S33, Supporting Information). Thereby all of the here measured Cd–OOC references showed approximately similar differences between the asymmetric and symmetric  $\text{COO}^-$  signal of 119, 115, 116  $\text{cm}^{-1}$  for Cd(oleate)<sub>2</sub>, Cd(myristate)<sub>2</sub>, Cd(acetate)<sub>2</sub>, respectively, fitting to the chelated/bidentate acetoacetate (<150  $\text{cm}^{-1}$ )<sup>[46]</sup> in the above mentioned literature study. This verifies the expected existence of a chelate and/or bidentate bond between the Cd of the OLA-NPLs and the carboxylate head group of the OLA.

On the contrary, for the not destabilized MUA-NPLs, the MUA was shown to preferably bind to the CdSe by a Cd–S–R species<sup>[26]</sup> and no bridging should occur. Thus, no such Cd–OOC bond should be present, which was confirmed by a significantly larger difference of 160  $\text{cm}^{-1}$ , resulting most probably from ionic  $\text{COO}^-$  species.<sup>[46]</sup>

If the hypothesis (4) of bridging neighboring NPLs through ligands bound via their two functional groups as Cd–S–(CH<sub>2</sub>)<sub>10</sub>–COO–Cd is true, the FTIR of the destabilized MUA-stacks should be different than that of the non-destabilized MUA-NPLs (were no bridging should be present). The MUA-stacks should show either the decreased distance between asymmetric and symmetric  $\text{COO}^-$  stretches when chelating or bridging is happening, as seen for the OLA-NPLs ( $\approx$ 120  $\text{cm}^{-1}$ ), or a very large difference when

monodentate bonds are present (>300  $\text{cm}^{-1}$ ).<sup>[46]</sup> In both cases when bridged by ligands it should be a different distance than for the non-bound MUA-NPLs sample. However, the distance for the MUA-stacks is still 160  $\text{cm}^{-1}$  so the same as for the MUA-NPLs. Therefore, this comparison verifies that no mentionable quantities of Cd–OOC bonds exists in the MUA-stacks and thus bridging of neighboring NPLs via Cd–S–(CH<sub>2</sub>)<sub>10</sub>–COO–Cd does not seem to be a prominent process in the MUA-stacks.

A different factor to consider would be the availability of free surface Cd atoms on the neighboring NPLs which would limit the possibility of bridging. At a high ligand coverage only a small percentage of surface Cd would be free to bind to the carboxylate end groups of ligands from the neighboring NPLs and thus, only a small percentage of ligands could bridge NPLs. Hence, the number of ligands should also be taken into account when considering bridging of NPLs and therefore, additional experiments were performed and are described in the following section.

### 2.3.5. Additional Purification Steps to Optimize Stacking Amount

It has been shown in our previous work, that a smaller amount of long aliphatic chained ligands on the NPL surface helps in the stacking process, due to easier intercalation of the steric ligands.<sup>[13]</sup> Additionally, bridging of ligands between neighboring NPLs can only occur, when there are available free Cd surface sites to bind to, as discussed in the previous section. Thus, an additional purification cycle of the MUA-NPLs was performed to reduce the amount of MUA ligands on the NPLs.

It is known from literature, that the additions of solvents such as EtOH could remove ligands from nanoparticle surfaces.<sup>[6]</sup> Here, ligand removal in the stacking procedure with THF was observed through XPS of the supernatant (MUA-stacks-supernatant, Figure 4; Figure S18, Supporting Information) which showed only signals of pure MUA ligands. This verifies the ability of THF to remove a certain amount of MUA ligands from the NPL surface. Therefore, the three times in a centrifuge filter washed MUA-NPLs were additionally precipitated with THF and redispersed in KOH followed by three more washing steps in a centrifuge filter (see experimental section). This additionally purified sample is called add.-purif.-MUA-NPLs in the following.

While the TEM images of the add.-purif.-MUA-NPLs already show a certain amount of stacking without any antisolvent addition (Figures S1 and S5, Supporting Information), the addition of THF as antisolvent leads to highly stacked NPLs even for small THF amounts (1:0.33  $V_{\text{NPLs}}:V_{\text{antisolvent}}$ , Figure 7; Figure S14, Supporting Information). This is also visible in the large hydrodynamic radii in the DLS measurements (Figure 7). As the amount of stacking is difficult to quantify through fallen over stacks and NPL laying on top of each other, the amount of stacking was tried to visualize in Figure S15 (Supporting Information). The number of NPLs in a stack varies from 2 NPLs to 38 with an average of  $7 \pm 4$  NPLs to the best of our measurement possibilities (Figure S16, Supporting Information). The additional precipitation step with THF thus leads to enhanced stacking of the NPLs, most probably through removal of ligands in the purification step. On the one hand, less ligands on the surface should reduce the charge repulsion of the NPLs and thus the stability in aqueous solution. Therefore, less antisolvent is necessary to

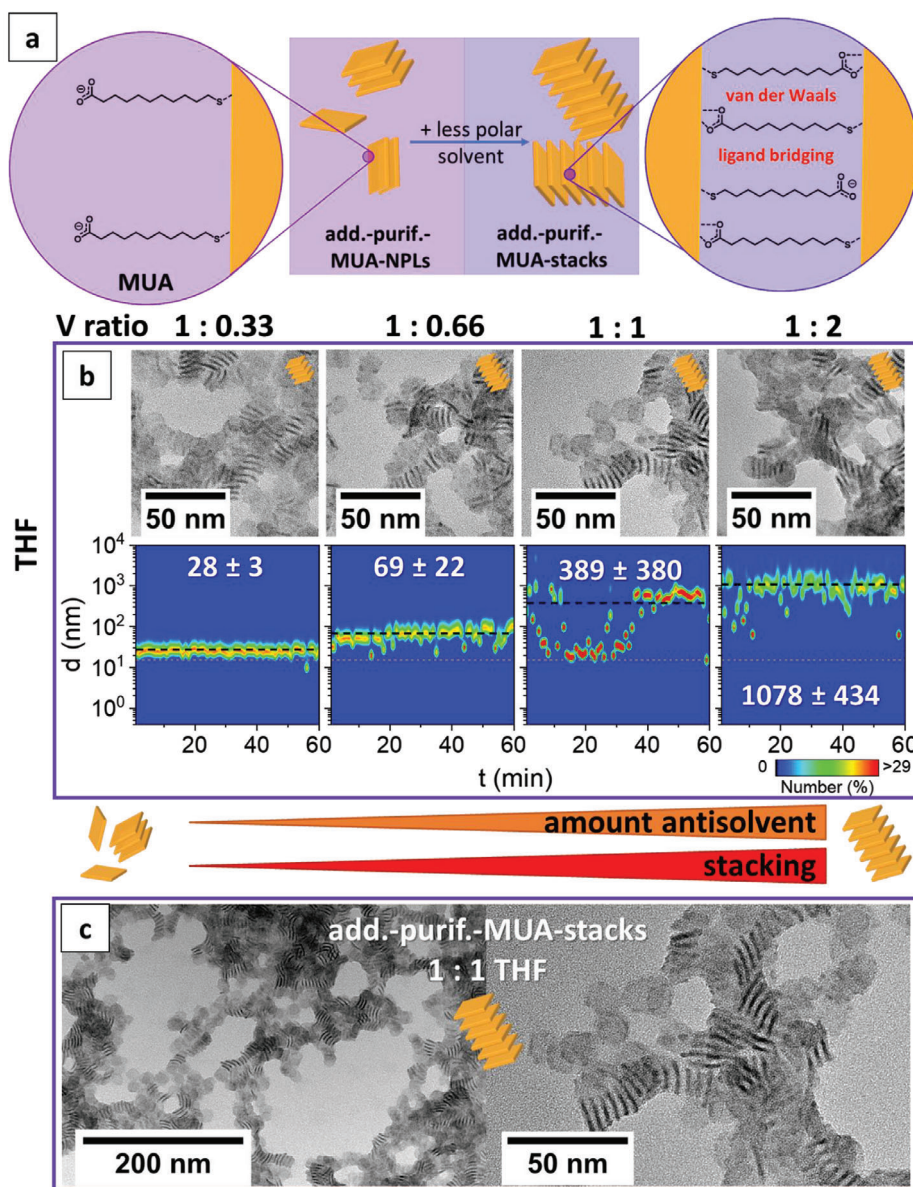


**Figure 7.** a) Schematic mechanism of the stacking of additional purified MUA-stacks. The smaller amount of MUA ligands on the surface enables easier intercalation of ligands and partial bridging of two NPLs via their MUA ligands. b) TEM micrographs and DLS measurements after different NPL to THF ratios (1:0.33, 1:0.66, 1:1, 1:2,  $V_{\text{NPLs}}:V_{\text{antisolvent}}$ ). The hydrodynamic size (derived by DLS) of the assemblies increases with antisolvent amount, while the add.-purif.-MUA-stacks show a high amount of stacking already for low THF ratios in the TEM micrographs. The mean values over 60 min of the add.-purif.-MUA-NPLs before THF addition (16 nm) is visible as grey dotted line and after THF addition as black dashed line. c) TEM micrographs in different magnifications of the add.-purif.-MUA-stacks after THF addition with a volume ration of 1:1 which can be seen as optimized stacked sample.

destabilize the add.-purif.-MUA-NPLs and initialize the stacking process. Additionally, the smaller number of charged carboxylate end groups would have more space to evade the other charged carboxylate end groups of the neighboring NPLs in the intercalation process and therefore lower the steric hindrance. On the other hand, the attractive van der Waals forces between the ligands should be reduced as less ligands should lead to less contact area and thus less possible interactions with neighboring molecules.<sup>[29,30,37]</sup>

In conclusion, the TEM images suggest, that the positive factors of a smaller number of ligands, such as the reduced steric

hindrance, outrank the negative factor of smaller van der Waals forces, leading to the enhanced stacking of the add.-purif.-MUA-NPLs.

Furthermore, less ligands on the NPL surface would not only enable easier intercalation of the electrosteric ligands, but also opens up the possibility of bridging of ligands between neighboring add.-purif.-MUA-NPLs, which was not seen for the normal MUA-NPLs, as discussed in the previous section. Inter-NPLs distances of the add.-purif.-MUA-stacks (1:1,  $V_{\text{NPLs}}:V_{\text{antisolvent}}$ ) were measured to be  $(1.5 \pm 0.2)$  nm from high resolution TEM images (55 measured, Figure S16, Supporting Information). This would

make ligand bridging possible, as fully stretched MUA ligands should have a length of 1.5 nm plus the radius of the head group calculated with the Tanford formula.<sup>[38]</sup>

To evaluate the bridging in the add.-purif.-MUA-stacks, again the FTIR is considered (Figure 6; Figure S30, Supporting Information). As written earlier, the difference between the asymmetric and symmetric COO<sup>-</sup> stretch can be considered to receive information about the binding situation of the carboxylate group.<sup>[45–47]</sup> For the MUA-NPLs and MUA-stacks the difference is 160 cm<sup>-1</sup> while the COO–Cd bound OLA-NPLs and COO–Cd containing references showed smaller differences between 120 and 115 cm<sup>-1</sup> (as analyzed in the previous section). In contrast, after the stacking, the add.-purif.-MUA-stacks show a difference between asymmetric and symmetric COO<sup>-</sup> stretches of 124 cm<sup>-1</sup> close to the references with COO–Cd bonds (Cd(oleate)<sub>2</sub>: 119 cm<sup>-1</sup>, Cd(myristate)<sub>2</sub>: 115 cm<sup>-1</sup>, Cd(acetate)<sub>2</sub>: 116 cm<sup>-1</sup>). Thus, a certain amount of Cd-S-(CH<sub>2</sub>)<sub>10</sub>-COO-Cd bridging of the add.-purif.-MUA-stacks through the MUA ligands via chelate and/or bidentate Cd–OOC bond seems to be highly probable when being stacked. The add.-purif.-MUA-NPLs without THF destabilization, which already show a certain amount of stacking in the TEM micrographs as described earlier, have a difference of 135 cm<sup>-1</sup> between the MUA-NPLs and the add.-purif.-MUA-stacks and thus most probably are a mixture of bridged and non-bridged NPLs.

In summary, the driving forces 1) of attractive van der Waals forces between the NPLs, 2) of the polarity difference between the antisolvent and ligands initializing the stacking through minimization of the contact areas of ligands and antisolvent, and 3) of the van der Waals forces between the intercalated ligands leading to ordered stacks, can be substantiated as essential for the stacking process. Instead, 4) bridging of NPL through ligands does not seem to occur in mentionable quantities for the standard used MUA-NPLs. However, the stacking can be improved by an additional purification step, most probably due to less ligands on the NPL surface leading to less charge repulsion and easier intercalation of the ligands in the stacking process and also enabling (4) the bridging for this add.-purif.-MUA-NPLs.

### 3. Conclusion

11-mercaptoundecanoic acid-capped CdSe nanoplatelets were successfully self-assembled into stacks from aqueous media. Thereby, the addition of antisolvents with lower polarity than methanol (such as tetrahydrofuran or ethanol) was shown to be efficient to initialize the stacking process. Here, dependencies of the stacking amount on the antisolvent amount and antisolvent polarity were found. The stacking increases with increasing antisolvent amount and with decreasing polarity. This was in good agreement to the known system of stacking in non-polar solvents where the stacking increases with increasing polarity of the antisolvent, meaning the larger the polarity difference between solvent and antisolvent the higher the destabilizing effect and thus the stacking in both cases. Thereby, the stacking process is a complex interplay of different repulsive and attractive interactions, which can furthermore change during the self-assembly. To simplify the discussion, four dominating driving forces of the stacking process in aqueous media were considered and examined through experiments. The first driving force determined was

the attractive van der Waals interaction between the flat plates of the NPLs, which is known to lead to agglomeration of nanoparticles when the repulsive interactions are too small to stabilize the nanoparticles in solution. The second driving force initializing the stacking process is the reduction of the repulsive electrosteric interactions of the ligands with the good solvent, which is known to change to attractive interactions through the addition of an antisolvent. This driving force can also be described as the minimization of the contact area between the antisolvent and ligands on the NPL surface. The antisolvent addition leads to intercalation of the surface 11-mercaptoundecanoic acid ligands (MUA) to minimize the contact area between the polar ligands and the non-polar antisolvent. Third, van der Waals forces between the intercalated long aliphatic ligands were identified as driving force being essential for the ordered assembly into stacks compared to non-ordered agglomeration. Thereby, ligands with short chain length (3-mercaptopropionic acid, MPA) were shown to be insufficient to stack the NPLs, most probably due to their weak van der Waals attraction. Fourth, bridging of neighboring NPLs through MUA ligands being bound to the NPLs via their two functional end groups forming a Cd-S-(CH<sub>2</sub>)<sub>10</sub>-COO-Cd bridge were considered. Here no large amount of bridging could be seen through FTIR measurements in the standard used MUA-stacks. However, the number of ligands was found to influence the stacking ability as well. Thus, an additional purification with a precipitation step to reduce the number of ligands on the surface was examined. Here, the additional purification led to enhanced stacking abilities of the NPLs (add.-purif.-MUA-stacks). A reduced number of ligands should not only be beneficial for the first driving forces, due to easier intercalation of the electrosteric ligands and less necessary antisolvent to destabilize the NPLs, but it also enables bridging through easier accessibility of surface Cd atoms. The FTIR indeed indicated a certain amount of bridging in the additional purified MUA-stacks.

In conclusion, this work showed not only a way to directly assemble CdSe-NPL into stacks in an aqueous solution, but also identified possible driving forces for the process. To gain a deeper understanding of the driving forces and the attractive and repulsive interactions in this aqueous system, molecular dynamic simulations could be beneficial in the future.

This new direct self-assembly of CdSe-NPL-stacks in aqueous media opens up multiple processes and methods, such as gelation,<sup>[16–19]</sup> photocatalysis,<sup>[21]</sup> sensing,<sup>[24]</sup> ink-jet printing<sup>[20]</sup> and photoelectrochemistry,<sup>[13]</sup> for future applications.

### 4. Experimental Section

**Reagents:** Sodium myristate (≥99%), methanol (MeOH, ≥99.8%), 1-octadecene (ODE, 90%), n-hexane (≥99%), cadmium acetate (99.995%), 11-mercaptoundecanoic acid (MUA, 95%), 3-mercaptopropionic acid (MPA, 99%) and ethanol (EtOH, ≥99.8%) were purchased from Sigma Aldrich. Cadmium nitrate tetrahydrate (99.999%), selenium (200 mesh, 99.999%), and oleic acid (OLA, 90%) were supplied by Alfa Aesar. Cadmium acetate dihydrate (98%) was purchased from ABCR. Tetrahydrofuran (THF, extra dry, 99.5%), acetonitrile (ACN, extra dry, 99.9%) were supplied by Acros. All chemicals were used as received without further purification.

**Synthesis of Cadmium Myristate:** Cadmium myristate was produced by following the description of a synthesis procedure described in

literature.<sup>[48]</sup> Namely, cadmium nitrate tetrahydrate (3221 mg) was dissolved in methanol (80 mL). At the same time sodium myristate (6262 mg) was dissolved in methanol (500 mL) through stirring for 1.5 h. Afterward the cadmium nitrate solution was added to the sodium myristate solution slowly. The white precipitate was filtered and washed with methanol (1.5 L) in a Buchner vacuum flask. The cadmium myristate was dried under vacuum for at least 12 h and stored in a glove box afterward.

**Synthesis of 4.5 ML Quasi-Quadratic CdSe-NPLs (called OLA-NPLs):** CdSe core NPLs with a quasi-quadratic shape and a thickness of 4.5 monolayers CdSe were synthesized following the description of a procedure previously published in literature.<sup>[6,12]</sup> Thereby, cadmium myristate (1360 mg), selenium (108 mg), and 1-octadecene (ODE, 120 mL) were mixed in a 250 mL three-neck round flask through a short period in an ultrasonication bath (10 s). The mixture was degassed for 30 min at 70 °C, purged with nitrogen and degassed again for 30 min at 70 °C. The reaction flask was set to 240 °C under a nitrogen flow. At 202 °C the septum was withdrawn and cadmium acetate dihydrate (640 mg) was added swiftly. The reaction was held at 240 °C for 8 min before oleic acid (4 mL) was injected. The solution was rapidly cooled with compressed air from the outside and more oleic acid (4 mL) was added around 160 °C. The reaction product was transferred to 4 centrifuge tubes. Ethanol (in total 50 mL) was added before centrifuging (4226 rcf, 10 min). The precipitate was redispersed in hexane (in total 60 mL) and centrifuged again (4226 rcf, 10 min). The supernatant was transferred to new centrifuge vials and precipitated with ethanol (in total 20 mL). The dispersion was centrifuged (4226 rcf, 10 min). The precipitate was redispersed in hexane (≈8 mL). The concentration was determined through atomic absorption spectroscopy. Those oleic acid capped quasi-quadratic CdSe-NPLs were called OLA-NPLs in the manuscript.

**Phase Transfer with 11-Mercaptoundecanoic Acid or 3-Mercaptopropionic Acid to Synthesize Mercaptocarboxylic acid Capped CdSe-NPLs (Called MUA-NPLs and MPA-NPLs):** The phase transfer was performed following a literature procedure with slight modifications.<sup>[26,49]</sup>

11-mercaptoundecanoic acid (34.8 mg) or 3-mercaptopropionic acid (13.9 μL) and KOH (20.5 mg) was dissolved in a methanol (2.5 mL) by ultrasonication, followed by addition of OLA-capped CdSe-NPLs in hexane (1.8 mL,  $c_{Cd} = 20$  mM). The two-phase system (OLA-NPLs in the top hexane phase) was shaken overnight in an orbit shaker. The successful phase transfer was visible through the orange color of the MeOH-KOH phase (bottom) and colorless hexane phase (top). The hexane phase was removed and the methanol phase was centrifuged (4226 rcf, 10 min) and the precipitate was redispersed in aqueous KOH (15 mL,  $10^{-2}$  M, pH 9). The dispersion was transferred to a centrifuge filter (100.000 MWCO) and centrifuged (2817 rcf, ≈8 min) followed by two more washing steps consisting of addition of 15 mL KOH each and centrifugation (2817 rcf, ≈8 min). The last centrifugation time was adjusted to yield ≈1.3 mL (to reach a NPL concentration slightly higher than  $c_{Cd}$  20 mM). The resulting MUA-NPLs / MPA-NPLs were stored under ambient conditions. The concentration was measured by Atomic Absorption Spectroscopy (AAS).

**Additional Purified 11-mercaptoundecanoic Acid Capped CdSe-NPLs (called add.-purif.-MUA-NPLs):** For the add.-purif.-MUA-NPLs this final MUA-NPL dispersion was precipitated with THF (1.2 mL, 4226 rcf, 10 min). The precipitate was redispersed in KOH (15 mL) and washed in a centrifuge filter (100.000 MWCO, 2817 rcf, ≈8 min). Fifteen milliliters KOH was added two more times followed by centrifugation in a centrifuge filter (100.000 MWCO, 2817 rcf, ≈8 min). The last centrifugation time was again adjusted to yield ≈1.3 mL add.-purif.-MUA-NPL dispersion.

**Stacking of NPLs:** The respective NPL dispersions were prepared to have a concentration of  $c_{Cd} = 19.57$  mmol L<sup>-1</sup> in their respective solvents (OLA-NPLs in THF, MUA-NPLs & MPA-NPLs in aqueous KOH  $10^{-2}$  M). Different volume of various antisolvents such as MeOH, EtOH, ACN, THF were added at a rate of 1 mL h<sup>-1</sup> with a syringe pump or by an Eppendorf pipet for small volumes. The used volume ratios were 1:0.33, 1:0.66, 1:1 and 1:2 ( $V_{NPLs}:V_{antisolvent}$ ) were the NPL volume was held constant. For example, to 75 μL of NPL solution (with a starting concentration of  $c_{Cd} = 19.57$  mmol L<sup>-1</sup>) 150 μL of antisolvent was added with 1 mL h<sup>-1</sup> to achieve a 1:2 ratio ( $V_{NPLs}:V_{antisolvent}$ ). For the smallest

ratio 1:0.33 ( $V_{NPLs}:V_{antisolvent}$ ), 25 μL of the antisolvent were added to 75 μL of the NPL dispersion (with a starting concentration of  $c_{Cd} = 19.57$  mmol L<sup>-1</sup>).

**Stacking of NPLs with Highest Amount of Stacking (add.-purif.-MUA-stacks):** The highest amount of stacking was achieved for the add.-purif.-MUA-NPLs with 1:1 NPLs to THF volume ratio ( $V_{NPLs}:V_{antisolvent}$ ). Here, the additional purified MUA-NPLs were prepared in an aqueous KOH ( $10^{-2}$  M) as described above with a cadmium concentration of  $c_{Cd} = 19.57$  mmol L<sup>-1</sup>. For 1:1 volume ratio 75 μL of this add.-purif.-MUA-NPL dispersion was transferred in a vial and 75 μL of THF was added with a syringe pump at a rate of 1 mL h<sup>-1</sup>. TEM was prepared by drop casting 10 μL of this solution directly on a TEM grid.

**UV-vis and Photoluminescence Spectroscopy:** UV-vis extinction spectra were recorded with a DualFL from Horiba Scientific in quartz cuvettes (path length 1 cm). Photoluminescence (PL) emission spectra were recorded in an Edinburgh FLS 1000 spectrometer. The samples were diluted in the according solvents.

**Atomic Absorption Spectroscopy:** Atomic absorption spectroscopy (AAS) was measured to determine the cadmium ion concentration of the NPL solutions. A Varian AA140 instrument equipped with an air/acetylene (1.5:3.5) flame atomizer was used. A certain amount of the NPL solution was dried in an air flow and afterward decomposed with 1 mL aqua regia overnight. The samples were diluted with Milli-Q water (18.2 MΩ cm). A calibration curve was obtained by measuring six standard solutions.

**Transmission Electron Microscopy:** Transmission electron microscopy (TEM) measurements were performed to investigate the amount of stacking after antisolvent addition as well as size distributions and inter-NPL distances. A Tecnai G2 F20 TMP from FEI equipped with a 200 kV field emission gun was used for all measurements. All samples were prepared by drop-casting the solution (5 μL – 10 μL) on carbon-coated copper TEM grids (Quantifoil, 300 mesh).

**Dynamic Light Scattering:** Dynamic light scattering (DLS) was measured to monitor the hydrodynamic size of the assemblies during the destabilization. DLS of the samples were measured in a Malvern Panalytical Zetasizer Nano ZSP with a 636 nm laser in backscattering mode. The samples were prepared in quartz cuvettes and measured for 1 h each, every measurement was taken through 12 runs of 5 s thus one measurement took 1 min.

**Infrared Spectroscopy:** Infrared spectroscopy was performed at a Bruker Tensor 27 in transmission mode (FTIR) or reflective mode (ATR). It was measured with a 4 cm<sup>-1</sup> resolution and the spectra were background corrected in an OPUS software. The samples were prepared by the previously described stacking procedure followed by addition of KBr. The samples were dried under vacuum in a glove box antechamber overnight. The dried samples were pressed into pellets for FTIR measurements using a pressing machine at 8000 kg weight. The pure cadmium references (cadmium acetate, cadmium myristate, and cadmium oleate) were measured in ATR mode directly without KBr addition.

**X-Ray Photo-Electron Spectroscopy:** X-ray photo-electron spectroscopy (XPS) was measured with PHI VersaProbe III with an Al 1486.6 eV mono at 25.2 W X-ray source. Survey spectra were measured with a pass energy of 224 eV (increment of -0.2 eV, 0.2 s per data point). High resolution spectra were measured with 27 eV as pass energy (increment of -0.05 eV, 2.4 s per data point) for different elements. A beam diameter of 100 μm was used. The samples were neutralized during the measurement with 1 V and 3 μA. The according sample solutions were drop-casted onto Si-wafers. For the MUA-stacks the destabilized solution was precipitated (4226 rcf, 1 min) to separate the stacks (precipitate) from free MUA-ligands in the supernatant. The precipitate and the supernatant were applied to Si-wafers separately. The analysis was performed using CasaXPS software<sup>[50]</sup> and all samples were charge corrected with the C1s signal for C-C binding at 284.8 eV.

## Supporting Information

Supporting Information is available from the Wiley Online Library or from the author.

## Acknowledgements

This work was supported by the German Research Foundation (Deutsche Forschungsgemeinschaft, DFG) under Germany's excellence strategy within the cluster of excellence PhoenixD (EXC 2122, project ID 390833453) and the grand BI 1708/4-3. R.T.G. and K.T. thank the Hannover School for Nanotechnology (hsn) for funding. D.D. would like to acknowledge the support by the German Research foundation (DFG research Grant DO 1580/5-1). The authors are thankful to the Laboratory of Nano and Quantum Engineering (LNQE) for providing the TEM facilities. Furthermore, the authors thank the German Research Foundation (Deutsche Forschungsgemeinschaft, DFG) for funding the XPS facilities (INST 187/789-1).

Open access funding enabled and organized by Projekt DEAL.

## Conflict of Interest

The authors declare no conflict of interest.

## Data Availability Statement

The data that support the findings of this study are available from the corresponding author upon reasonable request.

## Keywords

aqueous media, nanoplatelets, stacking, self-assembly

Received: May 17, 2023

Revised: August 15, 2023

Published online:

- [1] S. Ithurria, B. Dubertret, *J. Am. Chem. Soc.* **2008**, *130*, 16504.
- [2] S. Ithurria, M. D. Tessier, B. Mahler, R. P. S. M. Lobo, B. Dubertret, A. L. Efros, *Nat. Mater.* **2011**, *10*, 936.
- [3] S. Ithurria, G. Bousquet, B. Dubertret, *J. Am. Chem. Soc.* **2011**, *133*, 3070.
- [4] A. Riedinger, F. D. Ott, A. Mule, S. Mazzotti, P. N. Knüsel, S. J. P. Kress, F. Prins, S. C. Erwin, D. J. Norris, *Nat. Mater.* **2017**, *16*, 743.
- [5] M. D. Tessier, L. Biadala, C. Bouet, S. Ithurria, B. Abecassis, B. Dubertret, *ACS Nano* **2013**, *7*, 3332.
- [6] B. Abécassis, M. D. Tessier, P. Davidson, B. Dubertret, *Nano Lett.* **2014**, *14*, 710.
- [7] B. Guzelurk, O. Erdem, M. Olutas, Y. Kelestemur, H. V. Demir, *ACS Nano* **2014**, *8*, 12524.
- [8] S. Jana, T. N. T. Phan, C. Bouet, M. D. Tessier, P. Davidson, B. Dubertret, B. Abécassis, *Langmuir* **2015**, *31*, 10532.
- [9] A. Antanovich, A. Prudnikau, A. Matsukovich, A. Achtstein, M. Artemyev, *J. Phys. Chem. C* **2016**, *120*, 5764.
- [10] S. Jana, M. de Frutos, P. Davidson, B. Abécassis, *Sci. Adv.* **2017**, *3*, 1701483.
- [11] R. Momper, H. Zhang, S. Chen, H. Halim, E. Johannes, S. Yordanov, D. Braga, B. Blülle, D. Doblus, T. Kraus, T. Kraus, M. Bonn, H. I. Wang, A. Riedinger, *Nano Lett.* **2020**, *20*, 4102.
- [12] J. F. Miethe, A. Schlosser, J. G. Eckert, F. Lübke, N. C. Bigall, *J. Mater. Chem. C* **2018**, *6*, 10916.
- [13] R. T. Graf, A. Schlosser, D. Zámbo, J. Schlenkrich, P. Rusch, A. Chatterjee, H. Pfnür, N. C. Bigall, *Adv. Funct. Mater.* **2022**, *32*, 2112621.
- [14] P. Schapotschnikow, R. Pool, T. J. H. Vlugt, *Nano Lett.* **2008**, *8*, 2930.
- [15] N. C. Bigall, C. Wilhelm, M. L. Beoutis, M. García-Hernandez, A. A. Khan, C. Giannini, A. Sánchez-Ferrer, R. Mezzenga, M. E. Materia, M. A. Garcia, F. Gazeau, A. M. Bittner, L. Manna, T. Pellegrino, *Chem. Mater.* **2013**, *25*, 1055.
- [16] J. L. Mohanan, I. U. Arachchige, S. L. Brock, *Science* **2005**, *307*, 397.
- [17] P. Rusch, D. Zámbo, N. C. Bigall, *Acc. Chem. Res.* **2020**, *53*, 2414.
- [18] D. Zámbo, A. Schlosser, P. Rusch, F. Lübke, J. Koch, H. Pfnür, N. C. Bigall, *Small* **2020**, *16*, 1906934.
- [19] A. Freytag, S. Sánchez-Paradinas, S. Naskar, N. Wendt, M. Colombo, G. Pugliese, J. Poppe, C. Demirci, I. Kretschmer, D. W. Bahnemann, P. Behrens, N. C. Bigall, *Angew. Chem., Int. Ed.* **2016**, *55*, 1200.
- [20] F. Lübke, J. F. Miethe, F. Steinbach, P. Rusch, A. Schlosser, D. Zámbo, T. Heinemeyer, D. Natke, D. Zok, D. Dorfs, N. C. Bigall, *Small* **2019**, *15*, 1902186.
- [21] J. Schlenkrich, F. Lübke-Warwas, R. T. Graf, C. Wesemann, L. Schoske, M. Rosebrock, K. D. J. Hindricks, P. Behrens, D. W. Bahnemann, D. Dorfs, N. C. Bigall, *Small* **2023**, *19*, 2208108.
- [22] J. F. Miethe, F. Lübke, J. Poppe, F. Steinbach, D. Dorfs, N. C. Bigall, *ChemElectroChem* **2018**, *5*, 175.
- [23] E. Lhuillier, J. F. Dayen, D. O. Thomas, A. Robin, S. Ithurria, H. Aubin, B. Dubertret, *Phys. Status Solidi Curr. Top. Solid State Phys.* **2016**, *13*, 526.
- [24] A. Schlosser, L. C. Meyer, F. Lübke, J. F. Miethe, N. C. Bigall, *Phys. Chem. Chem. Phys.* **2019**, *21*, 9002.
- [25] J. Qu, P. Rastogi, C. Gréboval, C. Livache, M. Dufour, A. Chu, S. S. Chee, J. Ramade, X. Z. Xu, S. Ithurria, E. Lhuillier, *ACS Appl. Mater. Interfaces* **2020**, *12*, 22058.
- [26] T. Kodanek, H. M. Banbela, S. Naskar, P. Adel, N. C. Bigall, D. Dorfs, *Nanoscale* **2015**, *7*, 19300.
- [27] S. Naskar, J. F. Miethe, S. Sánchez-Paradinas, N. Schmidt, K. Kanthasamy, P. Behrens, H. Pfnür, N. C. Bigall, *Chem. Mater.* **2016**, *28*, 2089.
- [28] B. Mahler, B. Nadal, C. Bouet, G. Patriarche, B. Dubertret, *J. Am. Chem. Soc.* **2012**, *134*, 18591.
- [29] M. A. Boles, M. Engel, D. V. Talapin, *Chem. Rev.* **2016**, *116*, 11220.
- [30] D. Kim, D. C. Lee, *J. Phys. Chem. Lett.* **2020**, *11*, 2647.
- [31] B. Derjaguin, *Kolloid-Zeitschrift* **1934**, *69*, 155.
- [32] G. Gabka, P. Bujak, K. Giedyk, K. Kotwica, A. Ostrowski, K. Malinowska, W. Lisowski, J. W. Sobczak, A. Pron, *Phys. Chem. Chem. Phys.* **2014**, *16*, 23082.
- [33] S. Y. Lee, M. T. Harris, *J. Colloid Interface Sci.* **2006**, *293*, 401.
- [34] S. Lalitha, P. T. Manoharan, *J. Electron Spectros. Relat. Phenomena* **1989**, *49*, 61.
- [35] R. C. White, R. Haight, B. D. Silverman, P. S. Ho, *Appl. Phys. Lett.* **1987**, *51*, 481.
- [36] E. Ebrahimi, M. Irfan, F. Shabani, Y. Kocak, B. Karakurt, E. Erdem, H. V. Demir, E. Ozensoy, *ChemCatChem* **2020**, *12*, 6329.
- [37] R. J. Ouellette, J. D. Rawn, in *Organic Chemistry*, Elsevier, San Diego, CA **2014**, p. 142.
- [38] C. Tanford, *J. Phys. Chem.* **1972**, *76*, 3020.
- [39] P. E. Laibinis, G. M. Whitesides, D. L. Allara, Y.-T. Tao, A. N. Parikh, R. G. Nuzzo, *J. Am. Chem. Soc.* **1991**, *113*, 7152.
- [40] J. F. A. Oliveira, T. M. Milão, V. D. Araújo, M. L. Moreira, E. Longo, M. I. B. Bernardi, *J. Alloys Compd.* **2011**, *509*, 6880.
- [41] S. Kumar, J. K. Sharma, *Mater. Sci.* **2016**, *34*, 368.
- [42] P. Thangadurai, S. Balaji, P. T. Manoharan, *Nanotechnology* **2008**, *19*, 435708.
- [43] A. Antanovich, A. W. Achtstein, A. Matsukovich, A. Prudnikau, P. Bhaskar, V. Gurin, M. Molinari, M. Artemyev, *Nanoscale* **2017**, *9*, 18042.

- [44] W. Premaratne, W. Priyadarshana, S. Gunawardena, A. A. P. De Alwis, *J. Sci. Univ. Kelaniya Sri Lanka* **2014**, *8*, 33.
- [45] W. K. Lewis, A. T. Rosenberger, J. R. Gord, C. A. Crouse, B. A. Harruff, K. A. S. Fernando, M. J. Smith, D. K. Phelps, J. E. Spowart, E. A. Gulians, C. E. Bunker, *J. Phys. Chem. C* **2010**, *114*, 6377.
- [46] G. B. Deacon, *Coord. Chem. Rev.* **1980**, *33*, 227.
- [47] J. E. Crowell, J. G. Chen, J. T. Yates, *J. Chem. Phys.* **1986**, *85*, 3111.
- [48] M. D. Tessier, P. Spinicelli, D. Dupont, G. Patriarche, S. Ithurria, B. Dubertret, *Nano Lett.* **2014**, *14*, 207.
- [49] A. Schlosser, J. Schlenkrich, D. Zámbo, M. Rosebrock, R. T. Graf, G. E. Cano, N. C. Bigall, *Adv. Mater. Interfaces* **2022**, *9*, 2200055.
- [50] N. Fairley, V. Fernandez, M. Richard-Plouet, C. Guillot-Deudon, J. Walton, E. Smith, D. Flahaut, M. Greiner, M. Biesinger, S. Tougaard, D. Morgan, J. Baltrusaitis, *Appl. Surf. Sci. Adv.* **2021**, *5*, 100112.